

Brownian Carnot engine

Ignacio A. Martínez^{†,1,2,*} Édgar Roldán^{†,1,3,4,‡} Luis Dinis^{4,5}
 Dmitri Petrov,¹ J. M. R. Parrondo,^{4,5} and Raúl A. Rica^{1,§}

¹*ICFO – Institut de Ciències Fotòniques, Mediterranean Technology Park,
 Av. Carl Friedrich Gauss, 3, 08860, Castelldefels (Barcelona), Spain.*

²*Laboratoire de Physique, École Normale Supérieure,
 CNRS UMR5672 46 Allée d'Italie, 69364 Lyon, France.*

³*Max Planck Institute for the Physics of Complex Systems, Nöthnitzerstrasse 38, 01187 Dresden, Germany.*

⁴*GISC – Grupo Interdisciplinar de Sistemas Complejos. Madrid, Spain.*

⁵*Departamento de Física Atómica, Molecular y Nuclear,
 Universidad Complutense Madrid, 28040 Madrid, Spain*

(Dated: February 11, 2022)

Carnot engine played a crucial role in the development of thermodynamics, setting a fundamental upper limit to the efficiency of a motor operating between two thermal baths. Nowadays, micromanipulation techniques make possible to explore the thermodynamics of small systems at scales where fluctuations cannot be neglected. Here, we report on an experimental realization of a Carnot engine with a single optically trapped Brownian particle as working substance. We fully characterize the thermodynamics of the engine when operating both in and out of equilibrium, observing that our device reaches Carnot efficiency for slow driving. We also report on the fluctuations of the finite-time stochastic efficiency, showing that Carnot efficiency can be surpassed in individual or ensembles of a few number of non-equilibrium realizations of the engine. We analyze the stochastic efficiency large deviation behaviour and find a minimum of the distribution which can provide information about the fundamental characteristics of the engine.

PACS numbers: 05.70.Ln, 05.40.-a 05.70.-a

Thermodynamics was developed in the XIX century using the Carnot engine as a building block. Carnot realized that the maximum efficiency η_C attainable by a thermal engine working between two reservoirs at different temperatures (hot, T_h , and cold, T_c) is a universal function of the temperatures $T_h > T_c$ [1]. This universality was used by Kelvin to define a fundamental scale of temperature, obeying $\eta_C = 1 - T_c/T_h$ [2], and by Clausius to introduce the concept of entropy and prove his celebrated theorem: the change of entropy along a cycle, defined as $\Delta S = -\sum_i Q_i/T_i$, where Q_i is the heat transferred from a thermal bath at temperature T_i to the system, is positive and vanishes only if the process is reversible. Years after, the Carnot cycle also played a prominent role in the development of finite time thermodynamics, when Curzon and Ahlborn obtained the efficiency at maximum power of an irreversible engine [3].

The Carnot cycle consists of two isothermal processes, where the working substance is respectively in contact with thermal baths at different temperatures T_h and T_c , connected by two adiabatic processes, where the substance is isolated from any thermal bath. An external parameter is changed in such a way that the whole cycle is carried out reversibly. Following this scheme, one could devise a progressing miniaturization of a Carnot engine and eventually reproduce the cycle with a single

Brownian particle. In fact, a variety of thermodynamic processes and even a complete Stirling cycle have been already implemented with single Brownian particles manipulated by optical tweezers [4–8]. Interestingly, at the micro scale the exchange of energy between the particle and its surrounding becomes stochastic and yet one can rigorously define work, heat, and efficiency, within the framework of the recently developed *stochastic thermodynamics* [9, 10].

The implementation of a Carnot cycle with a single Brownian particle has remained elusive due to the difficulties of implementing an adiabatic process. Isolating a single particle from the surrounding fluid is experimentally challenging. A more feasible strategy is to simultaneously change the temperature and the external parameter in such a way that the entropy of the particle stays constant, but the necessary fine tuning of the temperature is an experimental challenge as well. Here we construct a Brownian Carnot engine putting forward an experimental technique that allows to precisely control both effective temperature and volume of a single microscopic particle [11–13]. The technique consists of a noisy electrostatic force on the particle that creates an effective thermal bath whose temperature can be increased from room temperature (no electrostatic force) up to hundreds or even thousands of Kelvins, far above the boiling point of water.

The working substance of our engine is a single optically trapped colloidal particle immersed in water [8]. For small displacements x from the trap equilibrium posi-

[†]These authors contributed equally to this work

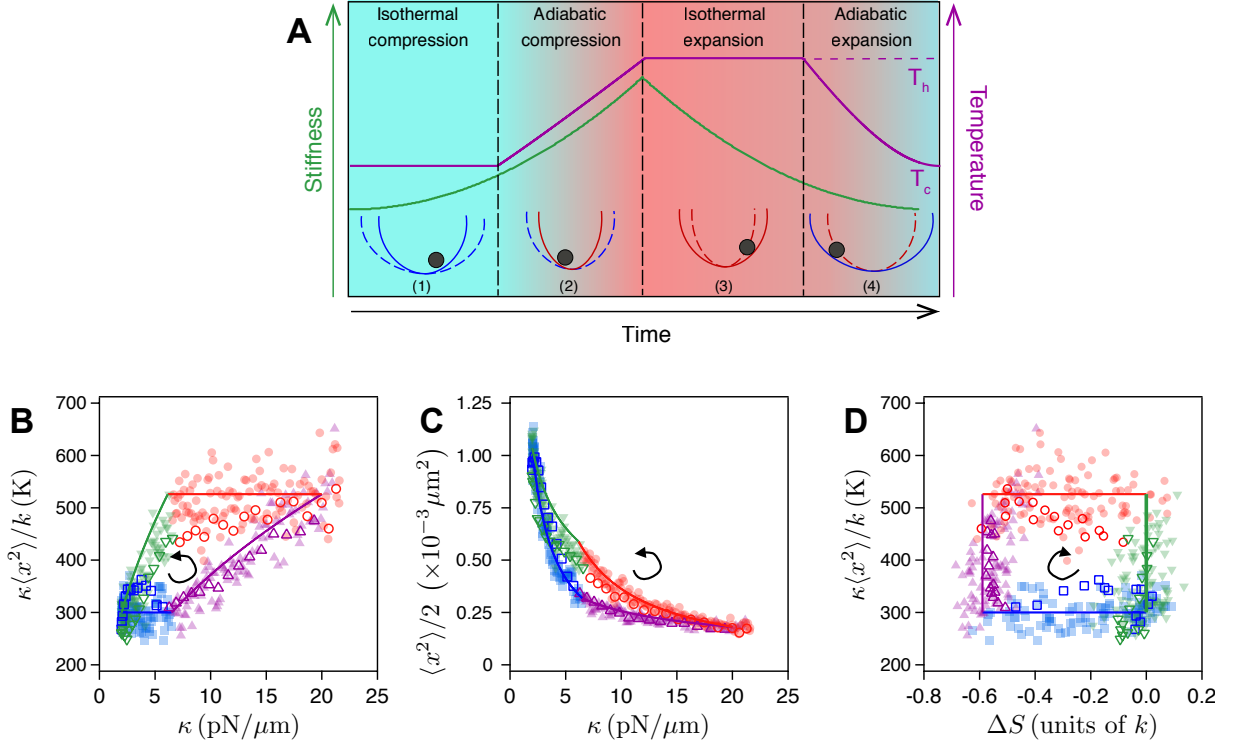


FIG. 1: The Brownian Carnot engine. (A) Sketch of the experiment. A single particle is confined in an optical trap with stiffness κ . The particle is subjected to an external random electric field that controls the temperature of the effective thermal bath T . Both κ and T can be arbitrarily managed using custom designed signals to implement the cycle with the desired duration. (B) Experimental protocol in the $T - \kappa$ plane, consisting of four processes: (1) Isothermal compression at $T = T_c$ (blue); (2) Adiabatic compression from $T = T_c$ to $T = T_h$ (magenta); (3) Isothermal expansion at $T = T_h$ (red); (4) Adiabatic expansion from T_h to T_c (green). Solid lines are the prescribed experimental protocols, the black arrow indicating the direction of the operation of the engine, while the output of our measurements is represented with symbols. Filled symbols are ensemble averages over series of cycles of duration $\tau = 200$ ms during $\tau_{\text{exp}} = 50$ s whereas open symbols correspond to ensemble averages over series of $\tau = 30$ ms cycles (corresponding to the engine operated at maximum power, see below) during $\tau_{\text{exp}} = 50$ s. In both cases the temperature of the particle is measured from the mean square displacement, $T_{\text{part}}(t) = \kappa(t) \langle x^2(t) \rangle / k$. (C) Clapeyron diagram (conjugated force $\langle x^2 \rangle / 2$ vs controllable parameter κ) of the engine obtained with the same durations of cycle. The area within the cycle is equal to the mean work obtained during the cycle. (D) T - S diagram. The entropy change is calculated as the difference between the Shannon entropy of the full phase space (position and velocity) at any time t and its value at the beginning of the cycle.

tion, the optical potential is harmonic and characterized by the trap stiffness κ , $U(x, t) = \kappa x(t)^2 / 2$. Here the trap stiffness plays the role of the control parameter as the volume of the piston does in classical thermodynamic engines. The Hamiltonian or total energy of the particle is $H(x, p; \kappa) = \kappa x^2 / 2 + p^2 / (2m)$, $p = m\dot{x}$ being the linear momentum of the particle. The conjugated force for κ is $F_\kappa(t) \equiv \partial H / \partial \kappa = x^2(t) / 2$, which is stochastic. As a result, the work necessary to implement a change $d\kappa$ in the external parameter, $dW(t) = F_\kappa(t) d\kappa$, and the heat or energy transfer from the thermal bath to the particle, $dQ(t) = dH(x(t), p(t)) - dW(t)$, are also fluctuating quantities.

As in standard thermodynamics, we first characterize the equilibrium states. The phase space density is $\rho_{\text{eq}}(x, p; \kappa, T) \equiv e^{-\beta H(x, p; \kappa)} / Z(\kappa, T)$, with $Z(\kappa, T) \equiv \int dx dp e^{-\beta H(x, p; \kappa)}$, $\beta = 1/(kT)$, k being Boltzmann's

constant. The equation of state reads $\langle F_\kappa \rangle_{\text{eq}} = \langle x^2 \rangle_{\text{eq}} / 2 = kT / (2\kappa)$ and the equation for the energy $E \equiv \langle H(x, p; \kappa, T) \rangle_{\text{eq}} = kT$, where the brackets denote average over $\rho_{\text{eq}}(x, p; \kappa, T)$. Next, we consider quasistatic processes where the system is in equilibrium at any stage of the process. In that case the average work is $\langle dW \rangle_{\text{eq}} = kT / (2\kappa) d\kappa$ and the average heat $\langle dQ \rangle_{\text{eq}} = kdT - kT / (2\kappa) d\kappa$. An adiabatic process is such that $\langle dQ \rangle_{\text{eq}} = 0$ and therefore $T(t)^2 / \kappa(t) = \text{constant}$. The adiabatic process can be equivalently defined as the process where the Shannon entropy of the particle $S_{\text{eq}} = -k \int dx dp \rho_{\text{eq}} \ln \rho_{\text{eq}}$ is constant.

We construct a Brownian Carnot engine with an optically trapped polystyrene particle of radius $R = 500$ nm concatenating the following processes (Fig. 1A and B): (1) *Isothermal compression* increasing κ from $\kappa_0 = (2.0 \pm 0.2)$ pN/ μ m to $\kappa_1 = (6.5 \pm 0.2)$ pN/ μ m, at constant ki-

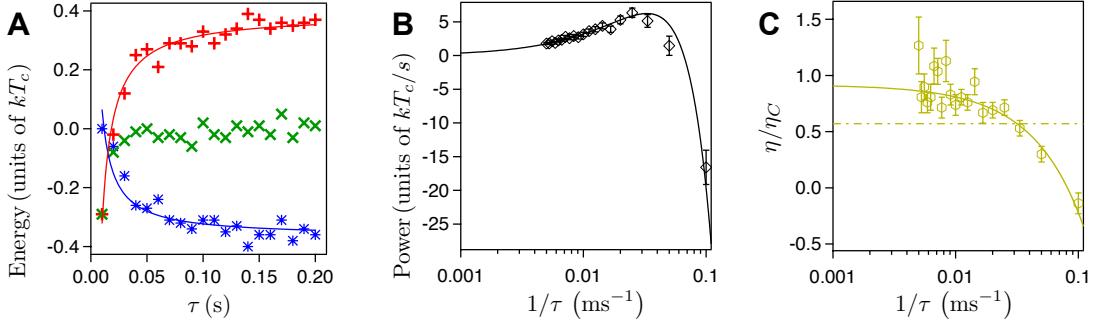


FIG. 2: **Energetics of the Brownian Carnot engine.** (A) Ensemble averages over $\tau_{\text{exp}} = 50$ s of stochastic work ($\langle W_\tau \rangle$, blue stars) and heat ($\langle Q_\tau \rangle$, red pluses) along one cycle as a function of the cycle duration. Green crosses are the average total energy change $\langle \Delta H_\tau \rangle$. Thin lines are fits to Sekimoto-Sasa law, $A + B/\tau$. (B) Power output $P = -\langle W_\tau \rangle/\tau$ as a function of the inverse of the cycle time (black diamonds). The black curve is a fit $P = (\langle W_\infty \rangle + \Sigma_{ss}/\tau)/\tau$, yielding $\langle W_\infty \rangle = (-0.378 \pm 0.008)kT_c$ and $\Sigma_{ss} = (5.7 \pm 0.3)kT_c \text{ ms}$ with a reduced chi-square of $\chi^2_{\text{red}} = 1.08$. (C) Efficiency of the engine as a function of the inverse cycle time (yellow hexagons). The solid yellow line is a fit of the efficiency to $\eta = (\eta_C + \tau_W/\tau)/(1 + \tau_Q/\tau)$, which yields $\eta_\infty = (0.92 \pm 0.06)\eta_C$, $\tau_W = (-11 \pm 2) \text{ ms}$, $\tau_Q = (-0.6 \pm 6.0) \text{ ms}$ with $\chi^2_{\text{red}} = 0.76$. Yellow dash-dot line is Curzon-Albourn efficiency $\eta_{CA} = 1 - \sqrt{T_c/T_h} = 0.25 = 0.57\eta_C$. Error bars are obtained with a statistical significance of 90%.

netic temperature $T = T_c = 300 \text{ K}$ (room temperature); (2) *adiabatic compression*, where the temperature of the bath is raised from T_c to $T_h = 525 \text{ K}$ while κ increases up to $\kappa_2 = (20.0 \pm 0.2) \text{ pN}/\mu\text{m}$ such that $T^2/\kappa = \text{const}$; (3) *isothermal expansion* at $T = T_h$ decreasing the stiffness from κ_2 to $\kappa_3 = (6.1 \pm 0.2) \text{ pN}/\mu\text{m}$; and (4) *adiabatic expansion* decreasing T from T_h to T_c while κ decreases back to κ_0 , keeping $T^2/\kappa = \text{const}$. The relaxation time of the particle is bounded from above by $\tau_r = \gamma/\kappa_{\min} = 4.2 \text{ ms}$, where $\gamma = 8.4 \text{ pN ms}/\mu\text{m}$ is the friction coefficient of the bead in water, obtained assuming Stokes Law. We explore the dynamics of the engine from the non-equilibrium regime, with short cycle time $\tau = 10 \text{ ms} \simeq 2\tau_r$, to the equilibrium one with long cycle time $\tau = 200 \text{ ms} \simeq 50\tau_r$. The cycle is repeated during $\tau_{\text{exp}} = 50$ s in all cases. The position of the bead is tracked with nanometric resolution at a sampling rate of 2 kHz. The stiffness and the kinetic temperature along the x -coordinate can be controlled with a resolution of $\Delta\kappa = 0.1 \text{ pN}/\mu\text{m}$ and $\Delta T = 1 \text{ K}$ and response times below milliseconds, allowing us to realize any thermodynamic protocol in the $T - \kappa$ plane (See Supplemental Information).

We measure different thermodynamic quantities (temperature, stiffness, heat, work and entropy) under both equilibrium and non-equilibrium driving (Figs. 1B-D). The effective temperature of the particle is obtained from the equipartition theorem for the potential energy, $T_{\text{part}}(t) \equiv \kappa(t)\langle x(t)^2 \rangle/k$, $\langle x^2(t) \rangle$ being the mean square displacement of the particle at time t . The $T - \kappa$ diagram of the engine (Fig. 1B) shows larger fluctuations in the quasistatic equilibrium protocol, which happens because the average is taken over a smaller number of cycles. In the non-equilibrium protocol, the most irreversible steps are the expansions, where the particle remains colder (i.e.

more confined [14]) than the environment. As in a macroscopic gas, the expansion is dominated by an entropic force, namely, the tendency of the gas to fill the available space. In the case of the single Brownian particle, the expansion is driven by thermal fluctuations that allow the particle to move farther away from the center of the trap. On the other hand, the compression is driven by the trap confining force, which allows the particle to react more rapidly and follow the equilibrium temperature even in fast cycles with $\tau = 30 \text{ ms}$ in the adiabatic compression. In the isothermal compression, however, we observe a fast initial increase of the temperature of the particle due to the increase of the stiffness. The $\langle x^2 \rangle - \kappa$ diagram (Fig. 1C) resembles Clapeyron pressure vs volume diagram of a Carnot cycle performed with an ideal gas [15].

The definition of stochastic entropy at the level of single trajectories allows to measure the entropy of a microscopic particle [16]. Here we measure the Shannon entropy of the particle at any time t averaged over all the cycles, $S(t) = -k \iint dx dv \rho(x, v, t) \ln \rho(x, v, t)$. Since the position and the velocity of the particle are uncorrelated, entropy is given by the sum $S(t) = S_x(t) + S_v(t)$, where $S_x(t) = -k \int dx \rho(x, t) \ln \rho(x, t)$ and $S_v(t) = -k \int dv \rho(v, t) \ln \rho(v, t)$, $\rho(x, t)$ and $\rho(v, t)$ being the marginal phase space densities calculated over x and v , respectively. Here, $\rho(x, t)$ is obtained from the statistics of trajectories that pass through x at time t along the experiment. To determine the velocity we extrapolate the time average velocity $v_{\Delta t}(t) = x(t + \Delta t) - x(t)$ using the technique described in [7]. The $T - S$ diagram of the particle (Fig. 1D) is a rectangle, where all the entropy change in the system occurs in the two isothermal steps. Taken all together, the thermodynamic diagrams under quasistatic driving (Figs. 1B-D) are equivalent to

those for a single particle ideal gas in a Carnot cycle [15].

During a cycle of duration τ , the working substance of the engine exchanges heat with the different thermal baths it is put in contact with, and under appropriate conditions it is able to extract work. We call W_τ and Q_τ the work exerted on the particle and the heat transferred from the environment to the particle along a cycle, respectively. The exchanged heat equals to $Q_\tau = \Delta E_\tau - W_\tau$, where $E = \kappa x^2/2 + p^2/(2m)$ is the total internal energy of the particle [9]. Both work and heat along the whole cycle (Fig. 2C) converge to their quasistatic averages $\langle \cdot \rangle_\infty$ following Sekimoto and Sasa's law $\langle W_\tau \rangle = \langle W_\infty \rangle + \Sigma_{ss}/\tau$ [17]. Here, $\langle W_\infty \rangle$ is the quasistatic value of the work done per cycle and the term Σ_{ss}/τ accounts for the (positive) dissipation, which decays to zero like $1/\tau$ [18]. In the case of the average heat per cycle, $\langle Q_\tau \rangle$, we find the dissipative term is negative, i.e., $\langle Q_\tau \rangle = \langle Q_\infty \rangle - \Sigma_{ss}/\tau$ with $\Sigma_{ss} > 0$ (Fig. 2A).

To quantify the performance of the engine, we analyze its power output and efficiency. First, we measure the power output as the mean total work exchanged during a cycle divided by the total duration of the cycle (Fig. 2B), $P = -\langle W_\tau \rangle/\tau$. For $\tau = 10$ ms, $\langle W_\tau \rangle$ is positive, the particle behaves as a heat pump and the power is negative. For larger values of τ the power increases, becoming positive, and eventually reaches a maximum value $P_{\max} = 6.34 kT_c/s$. Above that maximum, P decreases monotonically when increasing the cycle length. The data of P vs τ fit well to the expected law $P = -(\langle W_\infty \rangle + \Sigma_{ss}/\tau)/\tau$.

We further determine the efficiency of the motor η for different cycle durations. At odds with the macroscopic case, a finite amount of heat may be exchanged between the system and its environment during individual adiabatic steps in a given realization of the cycle, even though the average over many cycles vanishes in the quasistatic limit (see Supplemental Information). If heat is exchanged during other steps different from isothermals, even if only due to fluctuations, it may be relevant to include the heat transferred in the adiabatic steps in the efficiency. We therefore introduce the following definition of efficiency, which includes the contributions to the exchanged heat of the two adiabatic steps in the denominator,

$$\eta = \frac{-\langle W_\tau \rangle}{\langle Q_{2,\tau} \rangle + \langle Q_{3,\tau} \rangle + \langle Q_{4,\tau} \rangle}. \quad (1)$$

In the quasistatic limit, $\tau \rightarrow \infty$, the heat in the adiabatic processes vanishes, $\langle Q_{2,\infty} \rangle = \langle Q_{4,\infty} \rangle = 0$, yielding $\eta \rightarrow \eta_C$. The extrapolated value of the efficiency we obtain for long cycles is very close to Carnot efficiency, $\eta_\infty = (0.92 \pm 0.06)\eta_C$, the error bars being purely statistical (Fig. 2C). The experimental value of the efficiency at maximum power, $\eta^* \simeq 0.30$, is close to the Curzon-Ahlborn expression for finite-time cycles $\eta_{CA} = 1 - \sqrt{T_c/T_h} \simeq 0.24$ [3].

The fluctuating nature of energy exchanges in Brownian heat engines gives rise to subtleties that can only be characterized by a stochastic efficiency [19]. To account for the fluctuations of the engine, we investigate the stochastic efficiency rather than the fluctuations of the work or entropy production [10, 20, 21]. We define $W_\tau^{(i)}$ as the sum of the total work exerted on the particle along $i \geq 1$ cycles of duration τ , and $Q_{\alpha,\tau}^{(i)}$ the sum over i cycles of the heat transferred to the particle in the α -th subprocess ($\alpha = 1, 2, 3, 4$). We use the following definition of stochastic efficiency,

$$\eta^{(i)} = \frac{-W_\tau^{(i)}}{Q_{2,\tau}^{(i)} + Q_{3,\tau}^{(i)} + Q_{4,\tau}^{(i)}}, \quad (2)$$

which converges to the standard efficiency defined in Eq. (1) as $i \rightarrow \infty$. The one-cycle stochastic efficiency $\eta^{(1)}$ is strongly affected by thermal fluctuations (Fig. 3A). We derive an analytical expression for the distribution of $\eta^{(1)}$ for large τ (see Supplemental material), which only depends on the experimental protocol (black curve in Fig. 3A). When summing over a large number of cycles ($i = 200$ cycles, Fig. 3B) the efficiency distribution is peaked close to η_C for quasistatic driving, with a width that increases when reducing the duration of the cycle. For fast, non-equilibrium driving, the distribution exhibits a tail towards negative values. Both in one-cycle and large cycle distributions we observe fluctuations of efficiency above Carnot even for quasistatic driving.

Out of equilibrium and for large number of cycles i , the distributions of the fluctuations of $\eta^{(i)}$, $\rho(\eta^{(i)})$, are characterized by a large deviation function (LDF), $J(\eta^{(i)})$, which verifies $\rho(\eta^{(i)}) \sim e^{-i\tau J(\eta^{(i)})}$ [22]. The shape of the LDF of the stochastic efficiency can give information about the equilibrium properties of the system from non-equilibrium fluctuations [23, 24]. We calculate the LDF of stochastic efficiency for fast driving of the cycle by extrapolating the fluctuations of efficiency from 1 to 200 cycles (see Fig. 3C and Supplemental Information). For fast driving ($\tau = 30$ ms and $\tau = 20$ ms) the LDF attains a global maximum at positive efficiencies. This maximum corresponds to the least likely value of the efficiency and is attained beyond Carnot efficiency (Fig. 3C), as predicted theoretically for time-asymmetric cycles [24].

Extending the frontiers of micro and nano machinery has allowed to design small-sized engines which are able to transform the heat transferred from thermal fluctuations into mechanical work. Here we have realized the first Brownian Carnot engine with a single microscopic particle as a working substance, and characterized both its mean behavior and its fluctuations. At slow driving, our engine attains the fundamental limit of Carnot efficiency. The maximum power performed by our engine is ~ 250 larger than that of previous micro-engines [4] and only one order of magnitude below the power developed by some biological molecular motors such as

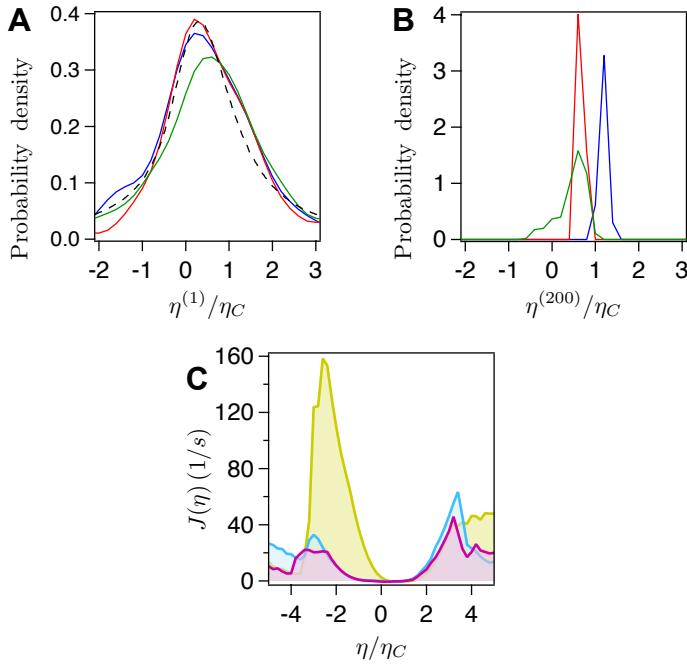


FIG. 3: **Efficiency fluctuations.** **A.** Distribution of $\eta^{(i)}$ calculated summing over $i = 1$ cycles of duration $\tau = 200$ ms (blue curve), $\tau = 100$ ms (red curve) and $\tau = 50$ ms (green curve) during $\tau_{\text{exp}} = 50$ s. The dashed black line is the theoretical distribution with no free parameter. **B.** Same for $i = 200$ cycles. **C.** Large deviation function of the efficiency for $\tau = 40$ ms (yellow shaded curve), $\tau = 30$ ms (cyan shaded curve) and $\tau = 20$ ms (magenta shaded curve).

Myosin motors [25]. The results of our experiment could be exploited in the design of novel biologically-inspired nano engines [26] and serve as energy supply for artificial nanorobots [27]. In vacuum, trapping techniques could benefit from our study of the efficiency fluctuations to build engines capable to outperform Carnot efficiency [28–30].

Acknowledgements: IAM, ER, DP and RAR acknowledge financial support from the Fundació Privada Cellex Barcelona, Generalitat de Catalunya grant 2009-SGR-159, and from the Spanish Ministry of Science and Innovation (MICINN FIS2011-24409). IAM acknowledge financial support from the European Research Council Grant OUTFELUCOP. ER acknowledges financial support from MPI-PKS. LD and JMRP acknowledge financial support from grant ENFASIS (FIS2011-22644. MINECO. Spanish Government). We wish to acknowledge the work of Stephen Corcuff at the earliest stage of the project and fruitful discussions with Ricardo Brito. Prof. D. Petrov passed away on 3 February 2014. He impulsed the development of this project while he was the leader of the Optical Tweezers group at ICFO. We mourn the loss of a great colleague and friend.

[†] Electronic address: edgar@pks.mpg.de

[§] Electronic address: rul@ugr.es

- [1] S. Carnot, in *Annales scientifiques de l'École Normale Supérieure* (Société mathématique de France, 1872), vol. 1, pp. 393–457.
- [2] E. Fermi, *Thermodynamics* (Dover, New York, 1956).
- [3] F. Curzon and B. Ahlborn, *Am. J. Phys.* **43**, 22 (1975).
- [4] V. Blickle and C. Bechinger, *Nature Phys.* **8**, 143 (2012).
- [5] E. Roldán, I. A. Martínez, J. M. R. Parrondo, and D. Petrov, *Nature Phys.* **10**, 457 (2014).
- [6] J. V. Koski, V. F. Maisi, J. P. Pekola, and D. V. Averin, *Proc. Natl. Acad. Sci.* **111**, 13786 (2014).
- [7] E. Roldán, I. A. Martínez, L. Dinis, and R. A. Rica, *Appl. Phys. Lett.* **104**, 234103 (2014).
- [8] I. A. Martínez, É. Roldán, L. Dinis, D. Petrov, and R. A. Rica, arXiv preprint arXiv:1409.7578 (2014).
- [9] K. Sekimoto, in *Lecture Notes in Physics, Berlin Springer Verlag* (2010), vol. 799.
- [10] U. Seifert, *Rep. Prog. Phys.* **75**, 126001 (2012).
- [11] I. A. Martínez, É. Roldán, J. M. R. Parrondo, and D. Petrov, *Phys. Rev. E* **87**, 032159 (2013).
- [12] P. Mestres, I. A. Martinez, A. Ortiz-Ambriz, R. A. Rica, and E. Roldan, *Phys. Rev. E* **90**, 032116 (2014).
- [13] A. Béruit, A. Petrosyan, and S. Ciliberto, *EPL (Europhys. Lett.)* **107**, 60004 (2014).
- [14] J. Gieseler, B. Deutsch, R. Quidant, and L. Novotny, *Phys. Rev. Lett.* **109**, 103603 (2012).
- [15] R. Feynman, R. Leighton, and M. Sands, *The Feynman Lectures on Physics*, vol. 1 (Addison-Wesley, Boston, 1963), 2nd ed.
- [16] U. Seifert, *Phys. Rev. Lett.* **95**, 040602 (2005).
- [17] K. Sekimoto and S.-i. Sasa, *J. Phys. Soc. Jap.* **66**, 3326 (1997).
- [18] M. V. S. Bonana and S. Deffner, *J Chem. Phys.* **140**, 244119 (2014).
- [19] K. Sekimoto, F. Takagi, and T. Hondou, *Phys. Rev. E* **62**, 7759 (2000).
- [20] C. Jarzynski, *Phys. Rev. Lett.* **78**, 2690 (1997).
- [21] G. E. Crooks, *Phys. Rev. E* **60**, 2721 (1999).
- [22] G. Verley, M. Esposito, T. Willaert, and C. V. den Broeck, *Nat. Commun.* **5**, 5721 (2014).
- [23] S. Rana, P. S. Pal, A. Saha, and A. M. Jayannavar, *Phys. Rev. E* **90**, 042146 (2014).
- [24] T. R. Gingrich, G. M. Rotskoff, S. Vaikuntanathan, and P. L. Geissler, *New J. Phys.* **16**, 102003 (2014).
- [25] J. Howard, *Mechanics of motor proteins and the cytoskeleton* (Sinauer Associates Sunderland, MA, 2001).
- [26] M. Sarikaya, C. Tamerler, A. K.-Y. Jen, K. Schulten, and F. Baneyx, *Nature Mat.* **2**, 577 (2003).
- [27] S. M. Douglas, I. Bachelet, and G. M. Church, *Science* **335**, 831 (2012).
- [28] J. Roßnagel, O. Abah, F. Schmidt-Kaler, K. Singer, and E. Lutz, *Phys. Rev. Lett.* **112**, 030602 (2014).
- [29] J. Gieseler, R. Quidant, C. Dellago, and L. Novotny, *Nature Nanotechnology* **9**, 358 (2014).
- [30] J. Millen, T. Deesuwana, P. Barker, and J. Anders, *Nature Nanotechnology* **9**, 425 (2014).

* Electronic address: martinez.ignacio@ens-lyon.fr